Using the Polymeric Ouzo Effect for the Preparation of Polysaccharide-Based Nanoparticles

ARTICLE *in* LANGMUIR · JUNE 2013

Impact Factor: 4.46 · DOI: 10.1021/la4017867 · Source: PubMed

Langmuir

Article

pubs.acs.org/Langmuir

Using the Polymeric Ouzo Effect for the Preparation of Polysaccharide-Based Nanoparticles

Eugen Aschenbrenner,[†] Karina Bley,[†] Kaloian Koynov,[†] Marcin Makowski,[†,‡] Michael Kappl,[†] Katharina Landfester,[†] and Clemens K. Weiss*[,†]

[†]Max-Planck-Institute for Polymer Research, Ackermannweg 10, 55128 Mainz, Germany

[‡]Institute of Physics, Poznan University of Technology, Nieszawska 13A, 60965 Poznan, Poland

Supporting Information

ABSTRACT: The polymeric ouzo effect, a nanoprecipitation process, is used for the preparation of polysaccharide-based nanoparticles. Dextran, pullulan, and starch were esterified with hydrophobic carboxylic acid anhydrides to obtain hydrophobic polysaccharides, which are insoluble in water. The additional introduction of methacroyl residues offers the possibility to cross-link the generated nanostructures, which become insoluble in organic solvents. To make use of the ouzo effect for the formation of nanoparticles, the polymer has to be soluble in an organic solvent, which is miscible with water. Here, acetone and THF were used. Immediately after the organic polymer solution is added to water, nanoparticles are generated. The size of the nanoparticles can be adjusted between 50 and 200 nm by changing the concentration of the initial polysaccharide solution. The degree of hydrophobic substitution was shown to have a very minor effect on the particle size. Dispersions with solids contents of up to 2% were obtained. Furthermore, the mechanical properties of the nanoparticles were investigated with force microscopy, and it was shown by fluorescence correlation spectroscopy that a fluorescent dye could be encapsulated in the nanoparticles by the applied nanoprecipitation procedure.

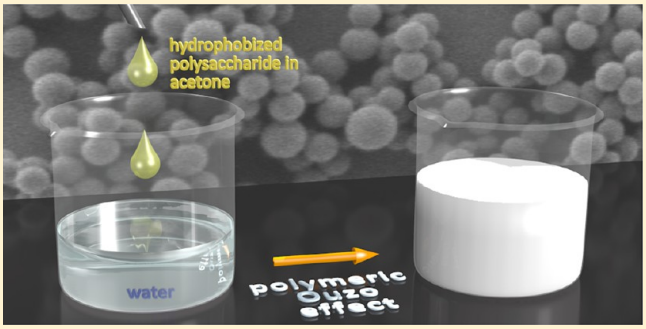

INTRODUCTION

Functional polymeric nanoparticles represent an important and actively researched class of materials. Their application in the biomedical sector as carriers for drugs or labels for cells and specific tissues is widely recognized.[1−3] Moreover, applications in fields as diverse as pigments[4] and modern lithography[5] are envisioned or already realized. Functional molecules or nanostructures can be chemically attached to the particle surface or incorporated into the polymeric matrix. Although surface modification is feasible on preformed particles with the appropriate chemical anchor groups (COOH, NH_2, OH, etc.), the incorporation of molecules or nanostructures is usually an integral part of the preparation process. Thus, especially for the encapsulation, powerful yet convenient and versatile preparation techniques are required.

Along with the classic technique of emulsion polymerization,[6,7] which in some cases can be used for the preparation of functional polymeric nanoparticles, the miniemulsion technique is an indispensable tool for the encapsulation of functional molecules and nanostructures in polymeric nanoparticles.[8]

However, particles made of some relevant polymers such as poly-L-lactide (PLLA) or polysaccharides are not accessible by (emulsion) polymerization methods. Thus, processes based on the precipitation of preformed polymers are the only way to formulate these polymers as (functional) nanoparticles. Precipitation of the polymer from a solution can be achieved by an increase in concentration, which is realized by solvent evaporation, the addition of a nonsolvent, or the evaporation of a solvent from a solvent/nonsolvent mixture. For controlled particle formation, a nucleus on which the polymer precipitates has to be provided. This can be a miniemulsion droplet[9] or inorganic nanoparticles to be encapsulated.[10] Confining the polymer solution to miniemulsion droplets and evaporating the solvent also leads to aqueous dispersions of nanoparticles.[11] Slow solvent exchange through dialysis membranes has been used by Heinze et al. for the preparation of polysaccharide-based nanoparticles.[12−14] The preparation of nanoparticles from synthetic polymers[15] or peptide polymer conjugates[16] has also recently been reported. Although mechanistically not completely understood, the so-called ouzo effect has been suggested and used for the preparation of polymeric nanoparticles.[17−20] Also referred to as nanoprecipitation or a solvent-shifting process, this phenomenon occurs when a solution of hydrophobic low-molecular-weight (such as anethol in ouzo) or high-molecular-weight compounds (such as polymers) dissolved in a water-miscible organic solvent as acetone or THF is added to excess water. Upon addition of the solution, a stable emulsion or

Received: May 12, 2013
Revised: June 18, 2013
Published: June 18, 2013

   dx.doi.org/10.1021/la4017867 | *Langmuir* 2013, 29, 8845−8855

dispersion with droplets or particles in the submicrometer range is generated. In addition to the formulation of pigments as microparticles or nanoparticles,[21−23] the process has predominantly been used in pharmaceutical sciences for the preparation of plain and drug-loaded polymeric particles[3,18] mainly from polyesters[24,25] but also from other polymers.[26−28] Because the emulsification/dispersion step does not require energy input, it is favorable for the application of sensitive polymers (polyesters) or the incorporation of sensitive materials (drugs) in polymeric particles.

In a typically very narrow area in the three-component phase diagram (water/solvent/polymer), nanophase separation is observed by introducing a solution of a water-insoluble compound in a solvent, which is miscible with water (acetone, THF, and acetonitrile) in excess water. Depending on the material used for dispersion, a surfactant is needed for the generation of long-term stable dispersions. Usually, without surfactant, the phases will slowly separate macroscopically to reach the thermodynamically stable state. However, if surfactant is used then the particle size is not affected by its presence. This indicates that the surfactant is not participating in the particle-formation process but rather just stabilizes the generated nanoparticles.

The ouzo effect is characterized by two very distinct features:[17,19,29,30] (1) The droplet or particle size depends on the concentration of polymer in the organic solution. Low concentrations lead to small particles, and higher concentrations produce large particles. The size distribution is narrow as long as the concentration is within the boundaries of the ouzo regime. (See item 2.) The initial step of particle formation is the spontaneous generation of nuclei, caused by the supersaturation of the polymer in the water/solvent mixture. According to the classical theory, the number of nuclei increases with higher supersaturation. If we assume that the particles grow by a nucleation-and-growth mechanism, particle growth is induced by material diffusion to and "precipitation" on the nuclei. Because more nuclei are present, this scenario leads to smaller particles at higher supersaturations, which is opposite to the situation described in the literature.[17,19,29,30] Alternatively, it has been proposed that the nuclei do not grow by diffusion but aggregate to form larger particles. Assuming a distinct volume, in which the nuclei aggregate, this process would indeed lead to larger particles at higher supersaturations, as more nuclei per volume unit are present at higher supersaturations. Most of the data presented in the literature support this mechanism.[17,19,29,30] However, it cannot be excluded that both processes occur simultaneously or sequentially. When working at high volume fractions of the solvent, diffusion of the polymer might occur. (2) Stable dispersions of uniform particles can be obtained only in a defined phase area that is located between the binodal and spinodal line in the miscibility gap.[17,19] The solids content of these dispersions is typically in the range of 1% or below. Attempts to prepare dispersions with higher concentrations lead to the formation of larger particles and eventually aggregates. The most intuitive explanation of spinodal decomposition was ruled out because the ouzo regime is not near the spinodal line in the phase diagram (at least for the investigated systems). The underlying mechanism is still unclear and the subject of ongoing research.

Here, we use the ouzo effect for the preparation of polysaccharide-based functional nanoparticles and present an evaluation of the mechanism of particle formation. Polysaccharides are very promising polymers for applications in nanotechnology.[12−14,31−35] They are ubiquitous in nature, and even nonfunctional polysaccharides such as dextran, starch, and pullulan can be very conveniently functionalized at their OH groups. They can be used for nucleophilic substitution, esterification, etherification, and reactions with epoxides or carbonyls. Thus, an extremely broad range of functionalities can be introduced, and the properties can be tailored according to the desired application. If aqueous dispersions of stable nanoparticles are to be prepared, the polymer has to be sufficiently hydrophobic in order to be insoluble in water. For this purpose, polysaccharides were hydrophobized by esterification with anhydrides of hydrophobic carboxylic acids. Additionally introduced methacroyl residues allow the cross-linking of the polymer. Because it is important for the evaluation of the ouzo mechanism, the degree of substitution with hydrophobic moieties was systematically varied to create a series of chemically comparable polymers with varying polarity. The possibility to incorporate functional molecules during particle generation was evaluated with a fluorescent dye using fluorescence correlation spectroscopy (FCS).

Furthermore, we used atomic force microscopy not only to characterize the topography of the particles in an aqueous environment but also to probe the mechanical properties (Young's modulus) of the particles.

MATERIALS AND METHODS

Materials. Dextran (35−40 kg·mol^{-1}), dimethylformamide (DMF) p.a., 2,2-dimethoxy-2-phenylacetophenone, fluorescein isothiocyanate (FITC, 90%) acetone p.a., and 2-propanol p.a. were purchased from Sigma-Aldrich; benzoic anhydride (98%) and triethylamine (99%) were purchased from Acros; potato starch and methacrylic anhydride (94%) were purchased from Fluka; hexanoic anhydride (99%) was purchased from Alfa Aesar; and LiCl was purchased from Carl Roth. Pullulan was kindly provided by Hayashibara Co., Ltd., Japan. All chemicals were used without further purification. Milli-Q-grade water was used throughout the experiments.

Preparation and Characterization of Modified Polysaccharides. Polysaccharides were esterified according to a protocol based on a publication by Kim et al.[36] In brief, the polysaccharide was dissolved in a 10 wt % LiCl solution in DMF at 90 °C. After the reaction mixture was cooled to 60 °C, an equimolar amount (with respect to the anhydride) of triethylamine was added, followed by the dropwise addition of methacrylic anhydride. The reaction was allowed to proceed for 2 h. To introduce additional hydrophobic residues, again triethylamine (equimolar to anhydride) and the respective anhydride were added (benzoic or hexanoic anhydride). The reaction was stopped after another 2 h by cooling to room temperature and precipitating in 2-propanol. The precipitate was separated by centrifugation (Sigma 3K30, 5 min, 10 000 min^{-1}), dissolved in acetone, precipitated in 2-propanol, and centrifuged again. Residual water-soluble products were removed by dissolving the crude product in acetone and by subsequent precipitation with water. Then, the product was dried in vacuum. The products were analyzed by ^{1}H NMR in DMSO-d_6. From the spectra, the degree of substitution (DS) was determined using eqs 1−3. A representative spectrum with assigned peaks is presented in the Supporting Information (Figure S1). The DS is given as residues per anhydroglucose unit (AGU), which is one-third of the residues/OH groups ratio. Dextran derivatives are labeled according to their functionalization and the degree of functionalization as follows: DexB_yMA$_x$ for dextran with benzoic and methacroyl residues and DexH_yMA$_x$ for dextran with hexanoic and methacroyl residues. Subscripts x and y depict the respective degrees of substitution:

$$\mathrm{DS[Dex}\mathbf{MA}\mathrm{]} = \frac{A[\text{olefinic}]@6.17\ \text{ppm}}{A[\text{anomeric}]@4.87\ \text{ppm}} \quad (1)$$

dx.doi.org/10.1021/la4017867 | Langmuir 2013, 29, 8845−8855

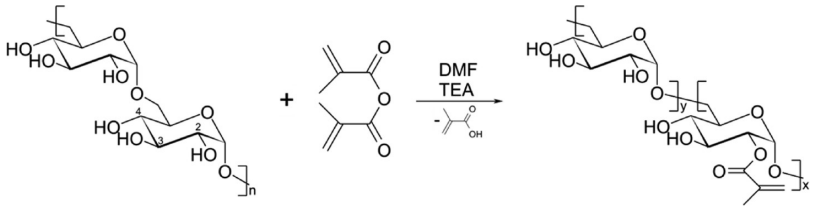

Figure 1. Reaction of dextran with methacrylic anhydride catalyzed by TEA.

$$\mathrm{DS[Dex\mathbf{B}MA]} = \frac{A[\text{aromatic}]@7.56\ \text{ppm}}{3A[\text{anomeric}]@4.87\ \text{ppm}} \quad (2)$$

$$\mathrm{DS[Dex\mathbf{H}MA]} = \frac{A[\alpha CH_2]@2.32\ \text{ppm}}{2A[\text{anomeric}]@4.87\ \text{ppm}} \quad (3)$$

The same strategy was used for the modification of pullulan and starch.

Fluorescence Labeling of the Polysaccharides with FITC. The hydrophobized polysaccharide (200 mg) was dissolved in DMSO (2 mL) and 30 μL of pyridine. After the solution was heated to 95 °C, FITC (11 mg) and dibutyltindilaurate (12 mg) were added. The mixture was allowed to stir for 2 h. Subsequently, the polymer was precipitated with *i*-propanol and centrifuged (Sigma 3K30, 5 min, 10 000 $\mathrm{min^{-1}}$). The supernatant was discarded, and the precipitate was dissolved in acetone. Then, the polymer was precipitated by the addition of water and again centrifuged. This procedure was repeated until the supernatant lost the characteristic yellow color of free fluorescein. After the sample was freeze-dried, a yellow powder was obtained.

Nanoparticle Formation. Different amounts of the modified polysaccharides ($\mathrm{DexB}_y\mathrm{MA}_x$, x = 0.23−0.26, y = 0.64, 0.84, 1.01 1.21, and 1.44) were dissolved in 2.5 g of acetone or THF to obtain concentrations from 1 to 60 $\mathrm{mg{\cdot}g^{-1}}$. These solutions were added to 5 g of Milli-Q water under vigorous stirring. Subsequently, the organic solvent was removed by holding at 40 °C overnight.

For the encapsulation experiments, modified FITC-labeled dextran was dissolved in acetone with fluorescent dye (Figure S2) (concentrations indicated in the text).

Cross-Linking. Cross-linking of the polymer was carried out under UV irradiation with a suitable UV initiator.[37] The nanoparticles were prepared using a 0.1 wt % solution of 2,2-dimethoxy-2-phenyl-acetophenone in acetone as the solvent for the dextran derivatives. A 100 W high-pressure Hg−UV lamp equipped with a 295 nm long-pass optical filter was used to irradiate the particle dispersion for 1 h.

The degree of cross-linking was determined by freeze-drying and redispersing the particles in acetone. After several cycles of acetone addition, redispersion, and removal of supernatant, the sediment and the combined supernatants were dried and the sol and gel contents were determined gravimetrically.

Particle Characterization. Particle sizes in the dispersion were determined by photon cross-correlation spectroscopy with a Nanophox PCCS (Sympatec). For the measurements, 50 μL of the dispersion was diluted in 2 mL of deionized water.

For the SEM measurements, 5 μL of the dispersion was diluted in 5 mL of deionized water and drop-cast on a silicon wafer. SEM images were taken at the 1530Gemini LEO (Zeiss) to determine the particle sizes in the dried state.

Fluorescence Correlation Spectroscopy. A commercial setup manufactured by Carl Zeiss (Jena, Germany) consisting of the ConfoCor 2 module and an Axiovert 200 inverted microscope was used. For all experiments, a Zeiss C-Apochromat 40×/1.2 W water-immersion objective was employed. The fluorophores were excited either with an argon laser at 488 nm or a HeNe laser at 633 nm. The emission was collected after filtering with LP505 or LP650 long-pass filters, respectively. Eight-well, polystyrene chambered coverglasses (Lab-Tek, Nalge Nunc International) were used as sample cells for aqueous dispersions of the fluorescent species with typical concentrations of few particles per femtoliter. For each solution, a series of 10 measurements with a total duration 5 min were performed. To determine the diffusion coefficients and hydrodynamic radii of the compounds, the measured autocorrelation curves were fitted to the model function[38]

$$(\tau) = 1 + \frac{1}{N}\left(1 + \frac{\tau}{\tau_D}\right)^{-1}\left(1 + \frac{\tau}{S^2\tau_D}\right)^{-1/2} \quad (4)$$

where N is the average number of fluorescent species in the observation volume V, τ_D is the lateral diffusion time, and $S = z_0/\omega_0$ is the ratio of axial to radial dimension of V. The diffusion coefficient of the fluorescent species D was determined as $D = \omega_0^2/4\tau_D$, and their hydrodynamic radius was determined through Stokes−Einstein equation $R_H = k_B T/6\pi\eta D$, where T is the temperature, k_B is the Boltzmann constant, and η is the viscosity of the solution. Furthermore, by dividing the average count rate by the average number of particles in the observation volume (N), we have determined the average fluorescence brightness of the species in kHz/particle. The calibration of the confocal observation volume was done using reference dyes with known diffusion coefficients (i.e., fluorescein and Alexa 647).

Atomic Force Microscopy. A commercial Veeco Multimode AFM with a Nanoscope IIIA controller (Bruker AXS, Santa Barbara, CA) with a standard tapping-mode liquid cell was used as a measurement setup. The topographic imaging and mechanical testing have been done on particles adsorbed on silicon wafers. The wafers, after cutting them to fit the microscope (10 × 10 $\mathrm{mm^2}$), were cleaned by cyclic sonication in acetone, ethanol, and Milli-Q water, followed by plasma treatment for 1 min. A drop of a diluted dispersion was placed on the piece of wafer to allow part of it to adsorb. After placing it on the microscope in the liquid cell, we filled the cell with MilliQ water and washed away the excess particle material. NP-type A cantilevers (Bruker AXS AFM Probes) with a resonance frequency of 8 ± 2 kHz (in aqueous solution) and an average spring constant of k = 0.35 ± 0.02 $\mathrm{N{\cdot}m^{-1}}$ (as determined by the thermal tune method)[39] were used after plasma treatment for 20 s to remove any organic contamination. The topographical images have been acquired to localize a single layer of particles on the surface for later mechanical testing. Once a proper particle was found, the AFM tip was located above its top, and at least 10−30 cantilever deflection versus piezo position curves were recorded to probe the mechanical properties using defined loads (1−10 nN). To calibrate the deflection sensitivity of the AFM (i.e., the conversion factor between the detector signal in volts and the cantilever deflection in nanometers), we recorded cantilever deflection versus piezo position curves on the hard silicon substrate as a reference. After subtracting the voltage offset obtained from fitting the zero force baseline, we converted the deflection voltage signal of each curve to force by dividing it by the deflection sensitivity and multiplying it by the spring constant of the cantilever. The distance is obtained by subtracting the cantilever deflection from the piezo position.[40,41] This conversion procedure was automatized using self-written software. The same software was used to calculate Young's modulus from measured force versus distance curves, which were fitted according to the Hertz model, and the apparent Young's modulus was determined for given sets of particles. The Hertz model describes the deformation of contacting spherical bodies with the assumption that the materials of the contacting bodies are homogeneous and isotropic, load causes only elastic deformations of a contact zone, the contact area is small in comparison to the surface area of the contacting bodies, and pressure forces are normal to a contact surface.[42,43]

dx.doi.org/10.1021/la4017867 | *Langmuir* 2013, 29, 8845−8855

RESULTS AND DISCUSSION

Preparation and Characterization of Polysaccharide Derivatives. Hydrophobic residues can easily be introduced into polysaccharides by esterification or etherification. Here, the polysaccharides were modified by triethylamine-activated esterification using carboxylic acid anhydrides. Subsequent addition of different anhydrides allows the introduction of multiple carboxylic residues. The general reaction scheme for dextran with an anhydride is illustrated by the reaction with methacrylic anhydride in Figure 1. The reactivity of the dextran OH groups in esterification reactions decreases from position 2 over position 3 to position 4.[44] Thus, esterification is likely to proceed preferably at the 2 position as indicated in Figure 1.

The first modification was the reaction with methacrylic acid anhydride to introduce the double bonds for later cross-linking. The degree of substitution (DS) with methacroylic residues can easily be assessed by comparing the integrals of the protons of the double bonds with the integral of the anomeric H of the anhydroglucose units (Supporting Information Figure S1). The DS for additional residues was determined by calculating the ratio of the integrals of the typical protons to the integral of the anomeric proton.

Figure 2 shows the dependence of the DS on the amount of anhydride used for the syntheses. The slopes indicate the

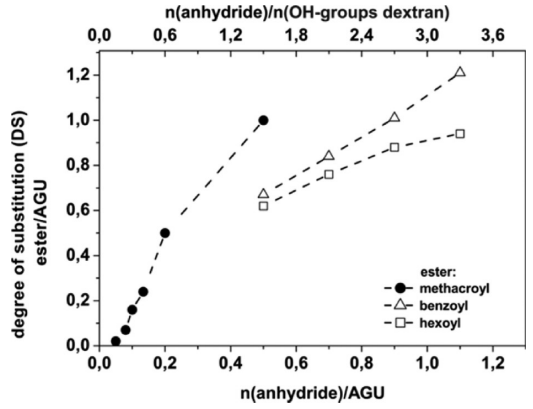

Figure 2. Variation of the DS using different molar ratios of the respective anhydride to hydroxyl groups of dextran. Dotted lines are guides to the eyes only.

reaction yields of the reactions with the respective anhydride. The highest reaction yield is obtained with methacrylic anhydride (72%), followed by benzoic anhydride (32%), and the lowest reaction yield was found using hexanoic anhydride (15%). Because the benzoic and hexanoic acid derivatives are prepared from an already modified dextran with a DS(MA) of approximately 0.2, the conversion might be lower as a result of the premodification. However, the DS of all modifications shows a linear relationship of the ratio of anhydride to glucose units. Therefore, it is possible to modify the polysaccharide selectively and adjust the DS.

Detailed studies were performed only with 40K dextran. However, the behavior of dextran with other molecular weights (500 000, 70 000, and 6000 g·mol^{-1}) as well as pullulan or starch is comparable.

For the preparation of nanoparticles, the polymers summarized in Table 1 were used. The hydrophobicity of the polymers is expressed by the HLB value. The higher the value, the less hydrophobic the polymer.

Table 1. HLB Values of the Modified Dextrans

DexB$_x$MA$_y$		
x	y	HLB
0.61	0.20	10.8
0.64	0.23	10.7
0.84	0.24	10.3
0.84	0.23	10.3
1.01	0.26	9.8
1.11	0.16	9.7
1.12	0.22	9.6
1.13	0.22	9.6
1.21	0.26	9.4
1.21	0.26	9.4
1.29	0.26	9.2
1.44	0.23	8.9
1.44	0.24	8.8
1.46	0.14	8.9
1.48	0.51	8.5
1.61	0.28	8.4
1.62	0.28	8.4

The HLB values were calculated according to the method of Davies using the increments published by Becher.[45] For pure dextran, an HLB value of 12.5 was calculated.

Nanoparticle Formation Using the Polymeric Ouzo Effect. *Overview.* The preparation of the modified polysaccharides and the particles can be conducted with dextrans of different molecular weights (500 000, 70 000, and 6000 g·mol^{-1}) and with several other polysaccharides such as pullulan and starch and several anhydrides (propionic anhydride and hexanoic anhydride) in the same manner. Micrographs of particles prepared from benzoylmethacroyl pullulan, benzoylmethacroyl starch, and hexylmethacroyl dextran are presented in Figure 3.

The samples underline the versatility of the process. However, detailed experiments were conducted with 40K DexBMA only because this polymer yielded the most uniform nanoparticles over a broad concentration range of up to 4 wt % polymer in the initial solution.

Influence of the Solvent. An appropriate solvent for the ouzo process has to dissolve the polymer, be miscible with water, and be easily removed from the dispersion. Typically, ethanol, acetone, or THF can be used. The solubility of the modified polysaccharides in ethanol is not sufficient, thus nanoparticles were prepared from acetone and THF solutions of DexBMA. Experiments with both solvents led to stable dispersions after the removal of the solvent. However, different particle sizes and size distributions were obtained for the same polymer concentrations. Additionally, the concentration range in which stable dispersions without macroscopic precipitation were obtained was different. Acetone solutions of up to 4 wt % could be used, whereas THF solutions of >2 wt % led to macroscopic coagulum. These differences are not surprising because the solubility of the polymers in the solvents is different and important parameters for phase separation, such as the diffusion coefficients and the viscosities, are different.

Surprisingly, the morphology of the nanoparticles prepared from THF solutions is spherical with one distinct cavity (Figure 4). In contrast, the particles prepared from acetone feature a "normal" spherical morphology, as visualized on the micrographs in Figure 3.

So as not to complicate the investigations with morphological issues, all additional experiments were conducted with acetone.

dx.doi.org/10.1021/la4017867 | Langmuir 2013, 29, 8845−8855

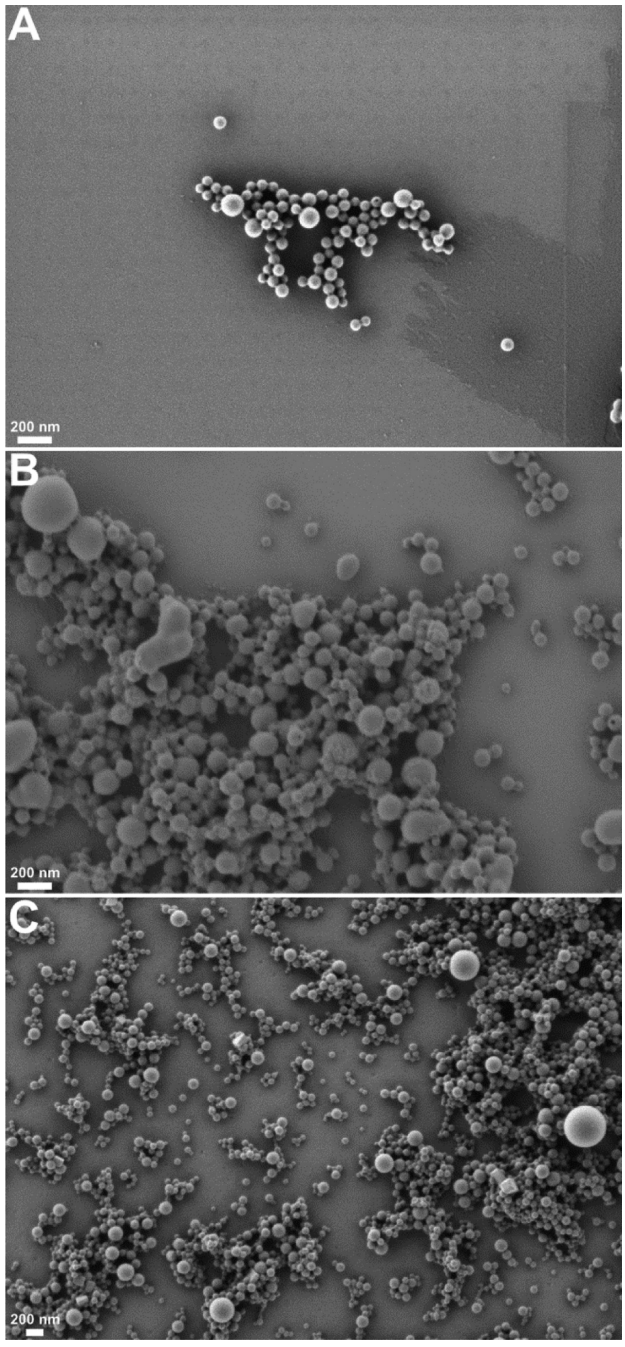

Figure 3. Scanning electron micrographs of particles from (A) benzoylmethacroyl pullulan, (B) benzoylmethacroyl starch, and (C) hexoylmethacroyl dextran, all prepared from acetone.

Stability. Interestingly, the dispersions are stable without the addition of surfactant, even for several months. Flocculated particles can easily be redispersed by simply shaking the dispersion. Table 2 shows the ζ potential of nanoparticles prepared from polymers covering the whole range of HLB values from 8.4 to 10.8. The concentration of the solution was 2 wt %. All of the values are around 0 mV, irrespective of the DS. This indicates that the particles are stabilized sterically.

Particle Sizes. Several parameters of the polymer (solution) have been reported to affect the particle size of colloids prepared by the ouzo effect, most notably the hydrophobicity of the polymer[24] and the concentration of the polymer solution.[18,30]

The hydrophobicity of the polymers has been adjusted by the degree of substitution and is expressed by the HLB value (Table 1). The polymer with the lowest HLB value is the most hydrophobic one. The hydrophobicity is mainly adjusted by the quantity of benzoyl substituents (x), and the DS of methacroyl residues (y) was kept in a very narrow range. Figure 4 shows the X_{50} particle diameter as a function of the concentration of the initial polymer solution and the DS of the polymer.

As can be seen from the graph in Figure 5, the particle size can be varied between 50 and 150 nm depending on the concentration. At higher concentrations, the particle sizes increased.

Aubry et al.[30] suggested a proportionality of the form $d \propto (c)^{1/3}$ for the dependence of the particle diameter (d) on the polymer concentration (c). A dependence of the diameter on the cubic root of the initial polymer concentration is consistent with the proposed aggregation mechanism. The number of nuclei increases linearly with the concentration of the initial solution. Thus, the volume of the aggregated particles also increases linearly with the concentration. This consequently means that the diameter increases with the cubic root of the concentration of the initial solution. To verify this model, the data were fit (Figure S3 in the SI) with a power law of the form $d = ac^b$, where d is the diameter, c is the concentration of the initial polymer solution, and a and b are the fitting parameters. It was found that parameter a is typically in the range of 80 nm·(g·L^{-1})$^{-b}$, with exponent b taking values from 0.28 to 0.39. Thus, the exponent is in the range expected for the above-described mechanism.

To investigate whether the ratio of polymer solution to water affects the particle size or size distribution, we prepared a solution of 20 mg·g^{-1} $DexB_{1.21}MA_{0.26}$ in acetone and added different amounts to 5 g of water. Figure 6 shows the particle sizes as a function of the amount of polymer introduced in the same concentration in acetone.

The particle size clearly shows no dependence on the amount of introduced polymer in the examined range. It underlines that the particle size indeed depends mainly on the initial concentration of the polymer solution. The results also indicate that the particles are unlikely to be created by a nucleation-and-growth mechanism. In this case, one would expect that the initially generated particles act as "seeds" on which new polymer precipitates when polymer solution is added dropwise.

In summary, all of the results obtained from the investigation of the particle sizes indicate that the nanoparticles are indeed generated by an aggregation of initially formed nuclei.

Cross-Linking and Swelling. Methacroyl residues were introduced into the polymer, which can be used for polymer cross-linking.[37] This is especially useful if the particles are to be dispersed in an organic solvent such as ethanol or acetone. Without cross-linking the particles would disintegrate because the polymer is soluble in polar organic solvents.

To be able to cross-link the polymer, we dissolved the polymer in acetone containing photoinitiator 2,2-dimethoxy-2-phenyl-acetophenone at low concentration (0.2 wt %). Irradiation with UV light cross-links the polymer after the particles have been generated by nanoprecipitation. These particles can be freeze-dried and redispersed in a polar organic solvent such as ethanol. Table 3 summarizes the particle sizes before and after cross-linking in water and after redispersion in ethanol. The particles listed are prepared from polymers with an equal DS of benzoyl residues and an increasing DS of methacroyl residues.

The particle size after cross-linking is slightly larger than before. The particles sizes before swelling are all in a narrow

dx.doi.org/10.1021/la4017867 | *Langmuir* 2013, 29, 8845−8855

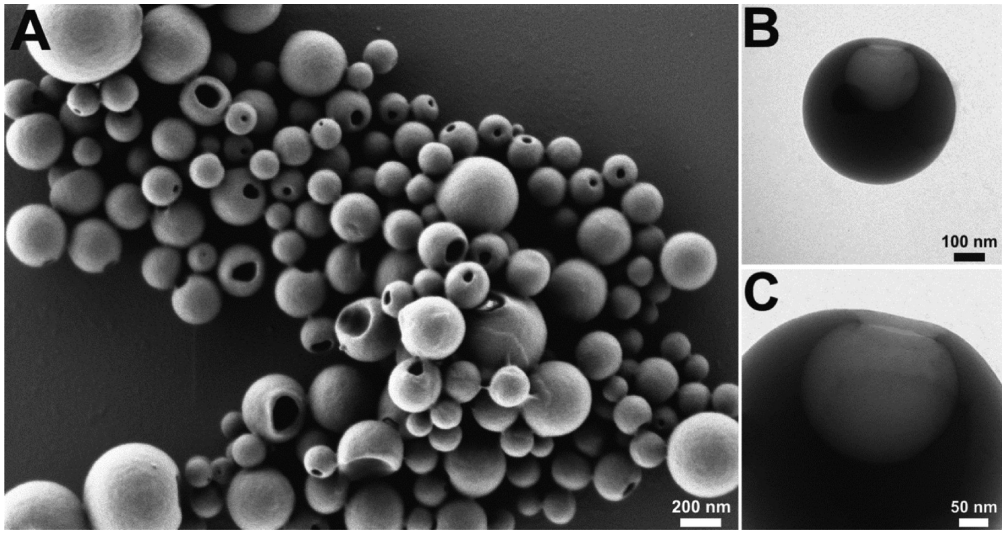

Figure 4. 40K DexBMA nanoparticles prepared from a THF solution. (A) The micrographs show the nanoparticles, each with one distinct cavity. (B, C) Transmission electron micrographs of a single particle with its cavity.

Table 2. ζ Potentials of Particles Prepared from Differently Functionalized DexBMA

$DexB_xMA_y$			
HLB	x	y	ζ potential (mV)
10.8	0.61	0.20	0.2
10.3	0.84	0.23	0.1
9.6	1.13	0.22	−0.2
9.2	1.29	0.26	−0.2
8.4	1.62	0.28	0.5

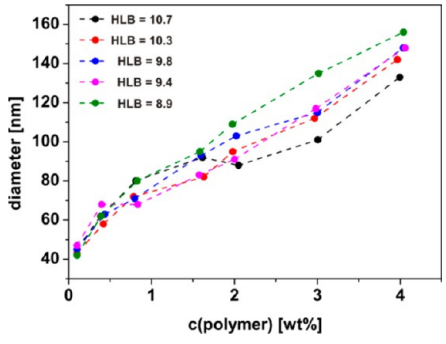

Figure 5. Particle size dependence on the initial concentration of the different polymers in acetone. The size was measured after the complete evaporation of acetone. Dotted lines are guides to the eyes only.

range, swollen in ethanol, and the particle size is largest for the particles prepared with the polymer of the lowest DS of MA and smallest for the particles prepared with the polymer of the highest DS of MA. The degree of swelling (Q = V(ethanol)/V(water)) underlines this trend (Table 3). It follows the expectation that in the case of a higher DS of MA more cross-linking points are present in the particle, thus the network is less flexible and cannot swell as much as with fewer connection points. The micrographs (Figure 7) underline that the particles are dissolved neither in acetone nor in ethanol and can thus be handled as dispersion in these organic solvents.

In addition, the sol/gel content of the dispersions was evaluated (Table 3). The freeze-dried particles were washed thoroughly with acetone to remove free, un-cross-linked chains

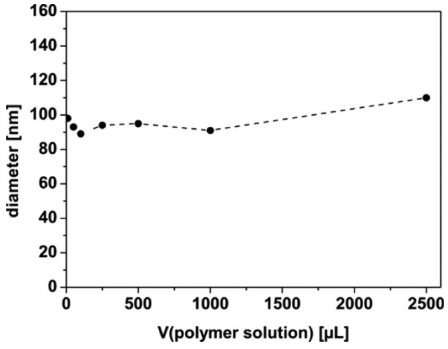

Figure 6. Dependence of the nanoparticle size on the volume of a $DexB_{1.21}MA_{0.26}$ solution (c = 20 mg·g^{-1}) dropped into 5 g of water. The dotted line is a guide to the eyes only.

Table 3. Particle Sizes, Degree of Swelling, Sol/Gel Amount of Particles after Cross-Linking[a]

	$DexB_xMA_y$		particle diameter (PCCS) (nm)					
HLB	x	y	before cross-linking	water	ethanol	degree of swelling	gel (%)	sol (%)
8.9	1.46	0.14	188	216	260	1.75	94	6
8.8	1.44	0.24	182	221	248	1.33	96	4
8.5	1.48	0.51	176	203	216	1.20	93	7

[a]DexBMA with different DS of MA was used: $DexB_{1.46}MA_{0.14}$, $DexB_{1.44}MA_{0.24}$, and $DexB_{1.48}MA_{0.51}$.

from the particles (sol). Irrespective of the DS of MA, the gel content is around 95%, which means that only 5% of the polymer is not incorporated into the network. Furthermore, even the lowest DS of MA is sufficient to entrap the polymer almost completely.

AFM Investigation and Mechanical Properties. Atomic force microscopy is a powerful tool that provides the ability to investigate particle morphology and measure mechanical properties on the nanoscale not only in air but also in a liquid environment, preventing the investigated material from collapsing as a result of drying and therefore probing the particles' properties in their "native" environment. Mechanical properties

dx.doi.org/10.1021/la4017867 | Langmuir 2013, 29, 8845−8855

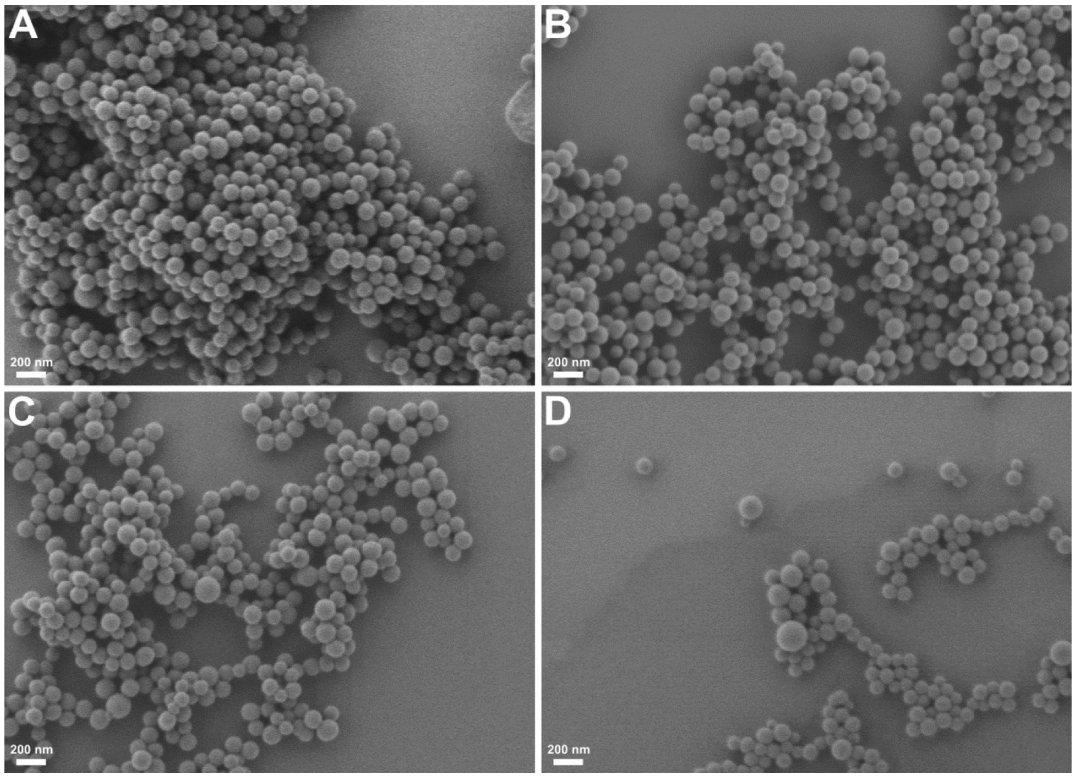

Figure 7. DexBMA nanoparticles: (A) before cross-linking, prepared from water, (B) after cross-linking, prepared from water, (C) after cross-linking, prepared from ethanol, and (D) after cross-linking, prepared from acetone.

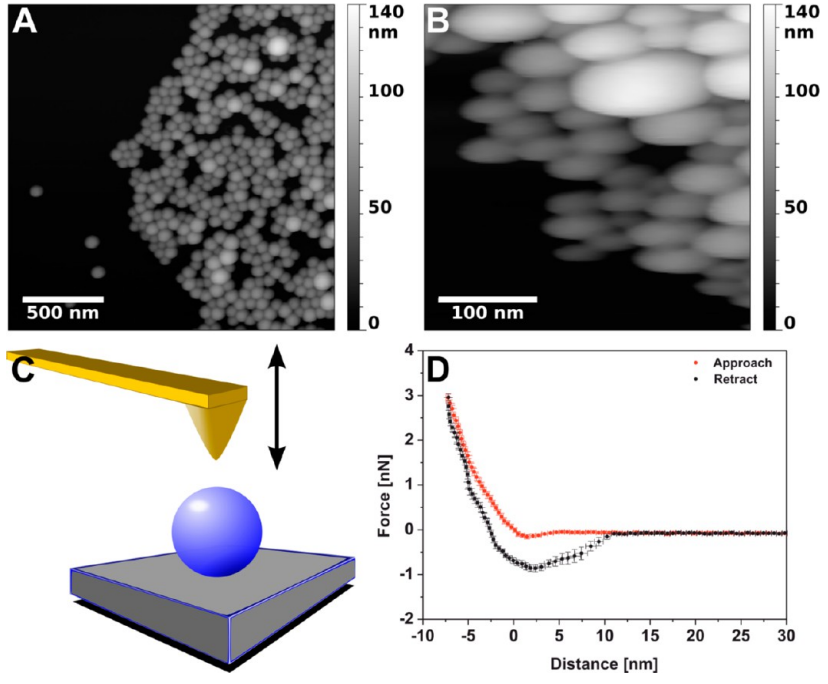

Figure 8. Typical AFM tapping-mode images of investigated samples. (A) HLB value of 10.3 and (B) HLB value of 10.7. (C) Schematics of the force spectroscopy experiment. (D) Exemplary force curve (averaged over nine repetitive measurements) for an HLB value of 10.3.

of colloids are interesting for several reasons. For example, it has been shown that polymeric particles made from low-T_g polymer are preferentially taken up by cells.[46] For the force microscopy investigations, particles made from modified dextran with four different HLB values were used. $DexMA_{0.1}$, with an HLB value of 12.4, was used for the preparation of cross-linked hydrogels, representing the most hydrophilic sample. Furthermore, DexBMA with HLB values of 10.7, 10.3, and 8.9 were used for the preparation of the nanoparticles. The sizes of the nanoparticles were all in the range of 100 nm. Figure 8A,B shows two representative AFM images (topography) of nanoparticles adhering to a silicon wafer, imaged under water.

dx.doi.org/10.1021/la4017867 | *Langmuir* 2013, 29, 8845−8855

They feature spherical morphology, comparable to what can be seen in electron micrographs. Figure 8C schematically shows the experimental setup of the mechanical measurements. After the AFM tip is placed above a chosen particle, the cantilever is approached to the particle and is then retracted again. This leads to force−distance curves, as shown in Figure 8d. The red curve shows the force during tip approach, and the black curve represents the force during retraction. From the curves, the Young's moduli can be calculated. These elastic moduli are shown in Figure 9, plotted versus the HLB of the polymer used for the preparation of the particles.

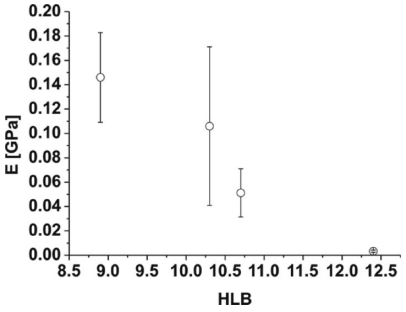

Figure 9. Elastic modulus of investigated particles made from modified dextran with different HLB values.

It is clearly visible that the modulus is highest for the particles prepared with DexBMA with an HLB value of 8.9 and lowest for the hydrogel (HLB value of 12.4). An almost linear relationship is visible. A possible reason might be that, with increasing HLB, the particles incorporate more water, reducing the elastic modulus. Because of the large experimental error and because there is no mechanistic model existing that would describe the relationship between HLB and elastic properties, the exact functional dependence is hard to predict. Linear, quadratic, or sigmoidal functions would all fit the data (but not exponential ones, see Supporting Information Figure S5). The values are in the range of those of lipid and polymeric vesicles.[40,47−51] Vesicles from egg yolk phosphatidylchloline have a Young's modulus of E = 2 MPa,[47,48] comparable to that of the hydrogel (E = 3 MPa) made from cross-linked dextran only. The particles from the most hydrophobic DexBMA have a modulus of E = 145 MPa, which is higher than that of vesicles from dipalmitoylphosphatidylcholine ($E \approx 100$ MPa).[49,51]

Investigation of Fluorescently Labeled Particles. Polysaccharides offer the possibility to functionalize the polymer conveniently with reactive fluorescent dyes such as fluoresceinisothiocyanate (FITC). Additionally, substances such as drugs and dyes can be incorporated into the nanoparticles by the ouzo effect. Both ways to prepare fluorescent nanoparticles were evaluated.

The modification of DexBMA with FITC is straightforward, despite the presence of the hydrophobic groups. It leads to an intensely fluorescing hydrophobic dextran derivative. For particle labeling, 2 wt % FITC-DexBMA was dissolved with DexBMA of the same DS in acetone and nanoprecipitated in water. A green fluorescing dispersion (Figure 10A) was obtained. In principle, the polymer can also be UV cross-linked, but the fluorescent dye suffers from serious photobloeaching. Thus, this procedure is suitable only for the preparation of un-cross-linked nanoparticles.

For encapsulation, a hydrophobic, highly photostable dye, BODIPY − B612-MA, has been added to the system for the nanoprecipitation procedure. The dispersion showed intense red

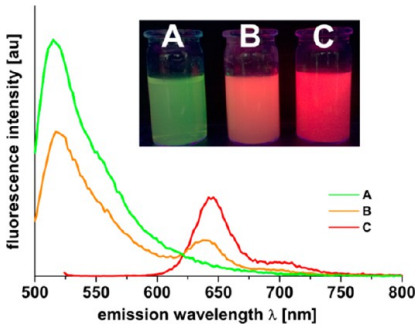

Figure 10. Photographs of fluorescing dispersions prepared with the polymeric ouzo effect during UV excitation (λ = 365 nm) and corresponding emission spectra of dispersions A−C. (A) FITC-$DexB_{1.12}MA_{0.22}$, (B) FITC-$DexB_{1.12}MA_{0.22}$ with encapsulated BODIPY dye, and (C) $DexB_{1.12}MA_{0.22}$ with encapsulated BODIPY dye.

fluorescence when irradiated with UV light (λ = 365 nm). Even after cross-linking, the fluorescence is visible (Figure 10C).

Finally, it is possible to encapsulate the BODIPY-based dye in a FITC-modified polymer. Here, the emissions of both dyes can be seen (Figure 10B).

Because the FITC and the BODIPY dyes have emission maxima, which are well separated from each other, the encapsulation of these dyes in the double-fluorescent labeled particles can be further investigated by fluorescence correlation spectroscopy (FCS).[52] The FCS technique is based on detecting the fluctuations of the fluorescent light intensity caused by the diffusion of fluorescent species through a small observation volume, usually formed by the focus of a confocal microscope. A correlation analysis of these fluctuations yields the diffusion coefficient and the hydrodynamic radius of the fluorescent species as well as their concentration and brightness (expressed in counts per particle).[38] Figure 11 shows the autocorrelation curves for the double-fluorescent labeled particles measured on the channels detecting the emission wavelength of FITC (Figure 11A) and of BODIPY (Figure 11B). For comparison, the autocorrelation curves obtained for dilute solutions of freely diffusing small dye molecules (fluorescein and Alexa 647) are also shown. Clearly, the dyes associated with the particles have smaller diffusion coefficients (the autocorrelation curves are shifted to longer lag times) than the free dyes.

By fitting the autocorrelation curves and using the Stokes−Einstein equation, the hydrodynamic radii of the fluorescent species in the dispersion can be calculated as R_h(FITC channel) = 50 nm and R_h(BODIPY channel) = 52 nm. These values correspond well to the radii of the nanoparticles obtained from PCCS (R_h = 65 nm), showing clearly that the FITC and BODIPY dyes are associated with the polymeric particles.

In addition to its simplicity, the described procedure for the hydrophobic dye encapsulation procedure also offers a straightforward way to tune the fluorescent brightness of the nanoparticles by adjusting the dye concentration in the initial solutions and thus the number of dye molecules per particle. To demonstrate this, we have prepared a series of fluorescent nanoparticles as summarized in Table 4. In all cases, 1 g of polymer/dye acetone solution was added to 2 g of water. The polymer concentration in the initial acetone solutions was 20 $mg \cdot mL^{-1}$ in all cases, but the dye concentration was systematically decreased from samples A1 and B1 to samples A3 and B3 (Table 4). Furthermore, two types of hydrophobic polysaccharides were used: A1−A3, samples with polymer with an HLB

dx.doi.org/10.1021/la4017867 | Langmuir 2013, 29, 8845−8855

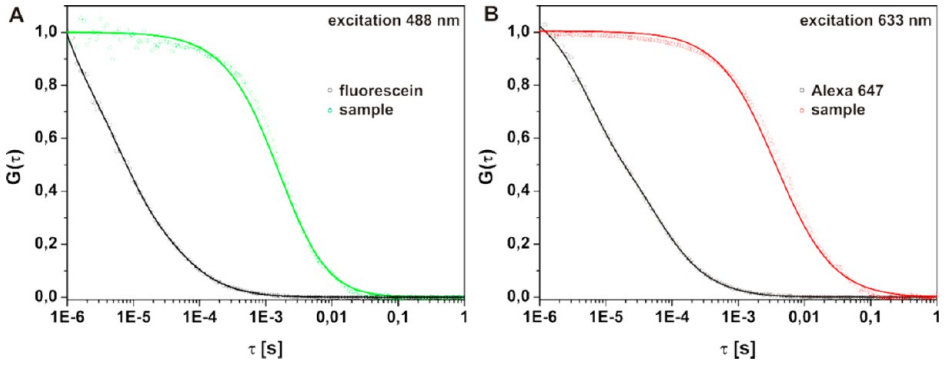

Figure 11. (A) Correlation curve of free dye fluorescein (black) and of fluorescein associated with the particles (green). (B) Correlation curve of free dye Alexa 647 (black) and of BODIPY associated with the particles (red).

Table 4. Characteristics of the Fluorescent Dispersions

	HLB = 9.7			HLB = 8.4		
	A1	A2	A3	B1	B2	B3
molar amount of dye conc (mmol)	1.8×10^{-5}	0.9×10^{-5}	0.36×10^{-5}	1.8×10^{-5}	0.9×10^{-5}	0.36×10^{-5}
diameter (nm)	145	153	159	156	149	169
brightness (kHz/part.)	40	21	10	46	22	11
N(dye/particle)	500	262	125	575	275	137
$N(\text{dye/particle})_{\text{theor}}$	865	508	228	1078	469	274

value of 9.7; B1−B3, samples with polymer with an HLB value of 8.4. The fluorescent brightness of these nanoparticles was measured with FCS, and the results are summarized in Table 4. It can be seen that the particle brightness increases almost linearly with the dye concentration in the initial acetone solutions. Finally, by measuring the brightness of the individual BODIPY molecules in dilute solutions of toluene (~0.08 kHz/molecule) and assuming that this value does not change significantly (e.g., because of quenching), we were able to estimate the average number of dye molecules per particle as shown in Table 4 when the dye molecules are encapsulated in the polymer nanoparticles. Although this number scales in the same way as theoretically estimated, its absolute value is somewhat lower than the theoretical value, which was calculated from the introduced amount of dye, the amount of polymer, and the diameter of the particles as determined by PCCS. The density of the particles was assumed to be 1.0 g·mL^{-1}. Several reasons may be named for the different values. (1) Although there was no visible precipitate of dye and no free dye detectable in FCS, the encapsulation efficiency is certainly not 100%. (2) The brightness of the free dye was measured in toluene, which is chemically comparable to the aromatic benzoyl residues of DexBMA but not identical. (3) Quenching of the encapsulated dye may also account for a reduced fluorescence intensity.

Furthermore, the particle sizes of the fluorescent particles were evaluated as a function of the polymer concentration of the initial solution. For the preparation, acetone-containing BODIPY at a concentration of 1.9×10^{-8} mol·g^{-1} was used. As already observed for the pure polymer system, the particle sizes increase with the concentration of the polymer in the initial solution. However, particles prepared with a comparable polymer without any fluorescent label have slightly smaller particle sizes.

CONCLUSIONS

Here, we have shown the synthesis of hydrophobized polysaccharides by the esterification of dextran, pullulan, or starch with methacrylic anhydride and other hydrophobic anhydrides. Making use of the polymeric ouzo effect, we prepared nanoparticles from these modified polysaccharides.

In particular, hydrophobic benzoylmethacroyl dextrans with a wide range of degrees of substitution were synthesized. Stable dispersions of polymeric nanoparticles were prepared by adding solutions of these polymers in acetone to water. The particle size shows a dependence of $d \propto (c)^{1/3}$ for any degree of substitution. This is in accordance with the proposed aggregation mechanism for particle formation with the polymeric ouzo effect. The polymer in the particles was cross-linked by UV irradiation, offering the possibility to disperse the nanoparticles in organic solvents such as ethanol and acetone.

Using atomic force microscopy in force spectroscopy mode, we investigated the mechanical properties. The Young's moduli of the particles were shown to correlate to the HLB value of the polymer, which was used for particle preparation.

Furthermore, it was shown by FCS that a fluorescent dye was embedded in the particles and the number of dye molecules in the particles can be adjusted by the amount of dye dissolved in the initial polymer solution.

In summary, we presented a convenient method for the preparation of functional nanoparticles from natural resources via a process requiring only minimal energy input.

ASSOCIATED CONTENT

Supporting Information

Example NMR spectrum, the structure of the BODIPY dye, the fits of the evolution of the particle size with the polymer concentration, additional AFM images, and possible fits for the elastic modulus versus HLB. This material is available free of charge via the Internet at http://pubs.acs.org.

AUTHOR INFORMATION

Corresponding Author

*E-mail: weiss@mpip-mainz.mpg.de. Tel: +49 6131 379581. Fax: +49 6131 379100.

Author Contributions

The manuscript was written through the contributions of all authors. All authors have given approval to the final version of the manuscript.

Notes

The authors declare no competing financial interest.

■ ACKNOWLEDGMENTS

We thank Dr. Andrey Turshatov for providing the BODIPY dye and Hayashibara Co. Ltd., Japan, for providing the pullulan. Gunnar Glaßer assisted during the acquisition of scanning electron micrographs, and Katrin Kirchhoff assisted during the acquisition of transmission electron micrographs.

■ REFERENCES

(1) Mailander, V.; Landfester, K. Interaction of Nanoparticles with Cells. *Biomacromolecules* **2009**, *10*, 2379−2400.
(2) Vauthier, C.; Bouchemal, K. Methods for the Preparation and Manufacture of Polymeric Nanoparticles. *Pharm. Res.* **2009**, *26*, 1025−1058.
(3) Mora-Huertas, C. E.; Fessi, H.; Elaissari, A. Polymer-Based Nanocapsules for Drug Delivery. *Int. J. Pharm.* **2010**, *385*, 113−142.
(4) Steiert, N.; Landfester, K. Encapsulation of Organic Pigment Particles via Miniemulsion Polymerization. *Macromol. Mater. Eng.* **2007**, *292*, 1111−1125.
(5) Vogel, N.; Weiss, C. K.; Landfester, K. From Soft to Hard: The Generation of Functional and Complex Colloidal Monolayers for Nanolithography. *Soft Matter* **2012**, *8*, 4044.
(6) van Herk, A. Historical Overview of (Mini)emulsion Polymerizations and Preparation of Hybrid Latex Particles. *Adv. Polym. Sci.* **2011**, *233*, 1−18.
(7) Bourgeat-Lami, E.; Lansalot, M. Organic/Inorganic Composite Latexes: The Marriage of Emulsion Polymerization and Inorganic Chemistry. *Adv. Polym. Sci.* **2011**, *233*, 53−123.
(8) Weiss, C. K.; Landfester, K. Miniemulsion Polymerization as a Means to Encapsulate Organic and Inorganic Materials. *Adv. Polym. Sci.* **2010**, *233*, 185−236.
(9) Paiphansiri, U.; Tangboriboonrat, P.; Landfester, K. Polymeric Nanocapsules Containing an Antiseptic Agent Obtained by Controlled Nanoprecipitation onto Water-in-Oil Miniemulsion Droplets. *Macromol. Biosci.* **2006**, *6*, 33−40.
(10) Prashant, C.; Dipak, M.; Yang, C. T.; Chuang, K. H.; Jun, D.; Feng, S. S. Superparamagnetic Iron Oxide - Loaded Poly(lactic acid)-D-α-tocopherol Polyethylene Glycol 1000 Succinate Copolymer Nanoparticles as MRI Contrast Agent. *Biomaterials* **2010**, *31*, 5588−5597.
(11) Schaeffel, D.; Staff, R. H.; Butt, H. J.; Landfester, K.; Crespy, D.; Koynov, K. Fluorescence Correlation Spectroscopy Directly Monitors Coalescence during Nanoparticle Preparation. *Nano Lett.* **2012**, *12*, 6012−7.
(12) Liebert, T.; Hornig, S.; Hesse, S.; Heinze, T. Nanoparticles on the Basis of Highly Functionalized Dextrans. *J. Am. Chem. Soc.* **2005**, *127*, 10484−10485.
(13) Hornig, S.; Heinze, T. Efficient Approach to Design, Stable Water-Dispersible Nanoparticles of Hydrophobic Cellulose Esters. *Biomacromolecules* **2008**, *9*, 1487−1492.
(14) Hornig, S.; Heinze, T. Nanoscale Structures of Dextran Esters. *Carbohydr. Polym.* **2007**, *68*, 280−286.
(15) Zhang, C.; Chung, J. W.; Priestley, R. D. Dialysis Nanoprecipitation of Polystyrene Nanoparticles. *Macromol. Rapid Commun.* **2012**, *33*, 1798−1803.
(16) Fuchs, A. V.; Kotman, N.; Andrieu, J.; Mailänder, V.; Weiss, C. K.; Landfester, K. Enzyme Cleavable Nanoparticles from Peptide Based Triblock Copolymers. *Nanoscale* **2013**, *5*, 4829−4839.
(17) Vitale, S. A.; Katz, J. L. Liquid Droplet Dispersions Formed by Homogeneous Liquid-Liquid Nucleation: "The Ouzo Effect". *Langmuir* **2003**, *19*, 4105−4110.
(18) Mora-Huertas, C. E.; Fessi, H.; Elaissari, A. Influence of Process and Formulation Parameters on the Formation of Submicron Particles by Solvent Displacement and Emulsification-Diffusion Methods Critical Comparison. *Adv. Colloid Interface Sci.* **2011**, *163*, 90−122.
(19) Ganachaud, F.; Katz, J. L. Nanoparticles and Nanocapsules Created Using the Ouzo Effect: Spontaneous Emulsification as an Alternative to Ultrasonic and High-Shear Devices. *ChemPhysChem* **2005**, *6*, 209−216.
(20) Miller, C. A. Spontaneous Emulsification: Recent Developments with Emphasis on Self-Emulsification. *Surf. Sci. Ser.* **2006**, *132*, 107−126.
(21) Van Keuren, E.; Georgieva, E.; Durst, M. Kinetics of the Growth of Anthracene Nanoparticles. *J. Dispersion Sci. Technol.* **2003**, *24*, 721−729.
(22) Van Keuren, E.; Bone, A.; Ma, C. B. Phthalocyanine Nanoparticle Formation in Supersaturated Solutions. *Langmuir* **2008**, *24*, 6079−6084.
(23) Horn, D.; Rieger, J. Organic Nanoparticles in the Aqueous Phase - Theory, Experiment, and Use. *Angew. Chem., Int. Edit.* **2001**, *40*, 4331−4361.
(24) Beck-Broichsitter, M.; Rytting, E.; Lebhardt, T.; Wang, X. Y.; Kissel, T. Preparation of Nanoparticles by Solvent Displacement for Drug Delivery: A Shift in the "Ouzo Region" upon Drug Loading. *Eur. J. Pharm. Sci.* **2010**, *41*, 244−253.
(25) Stainmesse, S.; Orecchioni, A. M.; Nakache, E.; Puisieux, F.; Fessi, H. Formation and Stabilization of a Biodegradable Polymeric Colloidal Suspension of Nanoparticles. *Colloid Polym. Sci.* **1995**, *273*, 505−511.
(26) Thioune, O.; Fessi, H.; Devissaguet, J. P.; Puisieux, F. Preparation of pseudolatex by nanoprecipitation: Influence of the solvent nature on intrinsic viscosity and interaction constant. *Int. J. Pharm.* **1997**, *146*, 233−238.
(27) Van Keuren, E. R. Polymer nanoparticles synthesized with solvent shifting. *J. Dispersion Sci. Technol.* **2004**, *25*, 547−553.
(28) Hornig, S.; Heinze, T.; Becer, C. R.; Schubert, U. S. Synthetic Polymeric Nanoparticles by Nanoprecipitation. *J. Mater. Chem.* **2009**, *19*, 3838−3840.
(29) Brick, M. C.; Palmer, H. J.; Whitesides, T. H. Formation of Colloidal Dispersions of Organic Materials in Aqueous Media by Solvent Shifting. *Langmuir* **2003**, *19*, 6367−6380.
(30) Aubry, J.; Ganachaud, F.; Addad, J. P. C.; Cabane, B. Nanoprecipitation of Polymethylmethacrylate by Solvent Shifting: 1. Boundaries. *Langmuir* **2009**, *25*, 1970−1979.
(31) Aumelas, A.; Serrero, A.; Durand, A.; Dellacherie, E.; Leonard, M. Nanoparticles of Hydrophobically Modified Dextrans As Potential Drug Carrier Systems. *Colloids Surf., B* **2007**, *59*, 74−80.
(32) Klinger, D.; Aschenbrenner, E. M.; Weiss, C. K.; Landfester, K. Enzymatically Degradable Nanogels by Inverse Miniemulsion Copolymerization of Acrylamide with Dextran Methacrylates as Crosslinkers. *Polym. Chem.* **2010**, *3*, 204−216.
(33) Heinze, T.; Liebert, T.; Heublein, B.; Hornig, S. Functional Polymers Based on Dextran. In *Polysaccharides II*; Klemm, D., Ed.; Springer: New York, 2006; Vol. *205*, pp 199−291.
(34) Oh, J. K.; Lee, D. I.; Park, J. M. Biopolymer-Based Microgels/Nanogels for Drug Delivery Applications. *Prog. Polym. Sci.* **2009**, *34*, 1261−1282.
(35) Boddohi, S.; Kipper, M. J. Engineering Nanoassemblies of Polysaccharides. *Adv. Mater.* **2010**, *22*, 2998−3016.
(36) Kim, S.-H.; Chu, C.-C. Synthesis and Characterization of Dextran-Methacrylate Hydrogels and Structural Study by SEM. *J. Biomed. Mater. Res. A* **2000**, *49*, 517−527.
(37) Hennink, W. E.; van Nostrum, C. F. Novel Crosslinking Methods to Design Hydrogels. *Adv. Drug Delivery Rev.* **2002**, *54*, 13−36.
(38) Rigler, R.; Elson, E. *Fluorescence Correlation Spectroscopy: Theory and Applications*. Springer-Verlag: Berlin, 2001.
(39) Hutter, J. L.; Bechhoefer, J. Calibration of Atomic-Force Microscope Tips. *Rev. Sci. Instrum.* **1993**, *64*, 1868−1873.
(40) Jaskiewicz, K.; Makowski, M.; Kappl, M.; Landfester, K.; Kroeger, A. Mechanical Properties of Poly(Dimethylsiloxane)-block-poly(2-methyloxazoline) Polymersomes Probed by Atomic Force Microscopy. *Langmuir* **2012**, *28*, 12629−12636.

(41) Butt, H.-J.; Cappella, B.; Kappl, M. Force Measurements with the Atomic Force Microscope: Technique, Interpretation and Applications. *Surf. Sci. Rep.* **2005**, *59*, 1−152.
(42) Burnham, N. A.; Colton, R. J. Measuring the Nanomechanical Properties and Surface Forces of Materials Using an Atomic Force Microscope. *J. Vacuum Sci. Technol., A* **1989**, *7*, 2906−2913.
(43) Ikai, A.; Afrin, R.; Sekiguchi, H.; Okajima, T.; Alam, M. T.; Nishida, S. Nano-mechanical Methods in Biochemistry Using Atomic Force Microscopy. *Curr. Protein Pept. Sci.* **2003**, *4*, 181−193.
(44) Vollmer, A.; Voiges, K.; Bork, C.; Fiege, K.; Cuber, K.; Mischnick, P. Comprehensive Analysis of the Substitution Pattern in Dextran Ethers with Respect to the Reaction Conditions. *Anal. Bioanal. Chem.* **2009**, *395*, 1749−1768.
(45) Becher, P. Hydrophile-Lipophile Balance: History and Recent Developments. *J. Dispersion Sci. Technol.* **1984**, *5*, 81−96.
(46) Lorenz, S.; Hauser, C. P.; Autenrieth, B.; Weiss, C. K.; Landfester, K.; Mailander, V. The Softer and More Hydrophobic the Better: Influence of the Side Chain of Polymethacrylate Nanoparticles for Cellular Uptake. *Macromol. Biosci.* **2010**, *10*, 1034−1042.
(47) Liang, X.; Mao, G.; Ng, K. Y. Mechanical Properties and Stability Measurement of Cholesterol-Containing Liposome on Mica by Atomic Force Microscopy. *J. Colloid Interface Sci.* **2004**, *278*, 53−62.
(48) Liang, X.; Mao, G.; Ng, K. Y. S. Probing Small Unilamellar EggPC Vesicles on Mica Surface by Atomic Force Microscopy. *Colloids Surf., B* **2004**, *34*, 41−51.
(49) Park, J. W. Sulfatide Incorporation Effect on Mechanical Properties of Vesicles. *Colloids Surf., B* **2010**, *80*, 59−62.
(50) Chen, Q.; Schönherr, H.; Vancso, G. J. Mechanical Properties of Block Copolymer Vesicle Membranes by Atomic Force Microscopy. *Soft Matter* **2009**, *5*, 4944−4950.
(51) Delorme, N.; Fery, A. Direct Method to Study Membrane Rigidity of Small Vesicles Based on Atomic Force Microscope Force Spectroscopy. *Phys. Rev. E* **2006**, *74*, 030901.
(52) Koynov, K.; Butt, H.-J. Fluorescence Correlation Spectroscopy in Colloid and Interface Science. *Curr. Opin. Colloid Interface Sci.* **2012**, *17*, 377−387.